



## Article

# Impact of Different Fixing Methods on the Vibration Characteristics of Single-Phase Transformers

Youliang Sun <sup>1,2</sup>, Yupu Sun <sup>2</sup>, Li Zhang <sup>1,\*</sup>, Liang Zou <sup>1</sup>  and Hao Wang <sup>1,\*</sup> 

<sup>1</sup> School of Electrical Engineering, Shandong University, Jinan 250061, China; 201920495@mail.sdu.edu.cn (Y.S.); zouliang@sdu.edu.cn (L.Z.)

<sup>2</sup> Shandong Power Equipment Company Limited, Jinan 250061, China; 18366040437@163.com

\* Correspondence: zhlee@sdu.edu.cn (L.Z.); 202120603@mail.sdu.edu.cn (H.W.)

**Abstract:** The vibration problem of single-phase transformers can threaten the stable operation of equipment, and long-term severe vibration may also cause mechanical fatigue or even damage to the equipment. Among these serious factors, the internal fixing method is one of the most important but easily overlooked factors, but the specific mechanism of the fixing method under different harmonics is still unclear. This article designs vibration and noise testing experiments for single-phase transformers, considering different harmonic excitations, as well as quantitatively compares and studies three different types of fixing methods: eccentric circle fixing, casting fixing, and pressure fixing. The effect of harmonic components on the vibration characteristics of single-phase transformers was studied, and the distribution characteristics of vibration and noise under different fixed methods were extracted and analyzed. The quantitative influence mechanism of fixed methods on audible noise was obtained.

**Keywords:** single-phase transformer; fixed method; vibration; noise; noise control



Academic Editors: Quanxin Zhu and Vasilis K. Oikonomou

Received: 10 December 2024

Revised: 3 January 2025

Accepted: 15 January 2025

Published: 21 January 2025

**Citation:** Sun, Y.; Sun, Y.; Zhang, L.; Zou, L.; Wang, H. Impact of Different Fixing Methods on the Vibration Characteristics of Single-Phase Transformers. *Symmetry* **2025**, *17*, 148. <https://doi.org/10.3390/sym17020148>

**Copyright:** © 2025 by the authors. Licensee MDPI, Basel, Switzerland. This article is an open access article distributed under the terms and conditions of the Creative Commons Attribution (CC BY) license (<https://creativecommons.org/licenses/by/4.0/>).

## 1. Introduction

Nowadays, with the accelerated development of human society, the contradiction between energy and the environment is intensifying, and the power load is rapidly increasing. Meanwhile, energy and load are often far apart, forcing high-voltage transmission technology to make faster progress [1–3]. Meanwhile, with the increasing awareness of environmental protection among people, the green development of transmission technology has become a core concern [4–7]. Among them, the vibration problems of transformers have become the main issue that urgently needs to be solved [8–11]. This may even threaten the safe and stable operation of the equipment, and increase energy loss and carbon emissions [12,13]. The noise problem of transformers is a long-standing and difficult-to-eliminate multidisciplinary issue, mainly caused by the magnetostriction effect and electrical vibration of internal components of transformer cores and windings under alternating electromagnetic fields. It is transmitted to the surface of the transformer tank in the form of vibration through a liquid medium transformer oil and a solid medium connection support structure, and finally diffuses into the surrounding air in the form of plane waves, forming a sound field domain centered on the transformer [14,15]. At present, there are two main methods to suppress transformer vibration noise, namely noise reduction in main components and structures, and noise reduction in partition absorption devices on the propagation path of vibration noise. The most fundamental and fundamental method is to directly suppress vibration from the structure [16,17]. Peng studied the influence of different harmonic operating conditions on the vibration characteristics

of transformers through simulation and experiments and proposed feasible solutions to suppress harmonic vibration. However, there was no further in-depth analysis of the component structure of transformers [18]. Janis proposed a modeling method to discuss the performance and distribution of the vibration characteristics of the three-phase three column transformer core, and theoretically proposed a new perspective for suppressing vibration in the core structure, but lacked sufficient experimental verification [19]. Based on the structural parameters and material properties of the fiber core, Li designed a model for the eddy current loss of the winding, which can quickly calculate the eddy current loss and can be used for the structural design [20]. Ji conducted a multi physics simulation study on the vibration and noise characteristics under different core structures, and derived the relationship between vibration noise and electromagnetic characteristics, but did not consider the differences between different excitation conditions [21]. Wang studied the impact of winding structure on the transformers, emphasizing the contribution of structure to resonance characteristics [22]. Wu proposed a frequency response method that can monitor the mechanical state of windings online, effectively extracting effective information on harmonic currents for transformer winding loosening faults in converters [23]. Chen conducted in-depth research on shielding technology in winding structures and found that shielding structures have significant effects in suppressing common mode noise [24]. He studied the transient potential distribution of transformer windings considering the influence of core laminations, and proposed the mechanism of the influence of laminations on the operating characteristics of the core and winding [25]. Zhu proposed a numerical vibration model for transformers that included damping effects, using the Rayleigh damping model to represent the damping effects of transformers. This model can be used to analyze methods for modal measurement that should not be implemented in engineering power transformers [26].

However, in terms of the current factory configuration of transformer manufacturers, most of the above studies have not yet been industrialized in the preparation of transformers [27,28]. This can be explained by the following two aspects: some studies have made progress in noise reduction, but have not considered the feasibility of transformer preparation [29]. Some studies have considered the feasibility of production, but it is difficult to strike a balance between noise reduction effectiveness and the economic viability of the results [30,31]. Particularly for the latter, transformer manufacturers are very concerned about the economic feasibility of equipment manufacturing materials. Improving the fixing method of transformers is an economical and feasible measure among the many noise reduction methods mentioned above [32]. However, currently, scholars have limited consideration and research on this denoising direction, making it difficult to form a comprehensive and unified set of fixed method selection criteria. We know that there is a significant difference between symmetric and asymmetric fixing methods in transformer modes, and the way fixing methods affect vibration characteristics mainly depends on the resonance effects caused by changing the mode. Therefore, it is particularly important to consider the operating conditions and harmonic components during the operation of transformers [33].

This article first introduces three different fixing methods from the aspects of design and structure and then presents an experimental platform for harmonic source and vibration noise testing system based on the single-phase experimental transformer provided by Shandong Electric Power Equipment Co., Ltd. Furthermore, a study was conducted on the impact of harmonic excitation on the vibration based on an experimental platform. Finally, a comprehensive study was conducted on the influence of symmetrical and asymmetrical fixed methods considering harmonics and working conditions on the characteristics of

single-phase transformers, and a quantitative comparative analysis was conducted on the audible noise under different fixed methods.

## 2. Mathematical Model of Vibration and Noise of Single-Phase Transformer

### 2.1. Core Vibration

The core composed of stacked silicon steel sheets undergoes magnetostrictive strain under the action of an alternating magnetic field, resulting in magnetostrictive force inside the core. Considering the anisotropy of the magnetostrictive force of the iron core,  $x$  is defined as the rolling direction of the stacked silicon steel sheets in the core,  $y$  is the magnetic field direction of the core, and  $z$  is a direction perpendicular to the magnetic field. Therefore, magnetic field intensity forces in different directions can be expressed separately.

$$f_x = \frac{\partial}{\partial x} \left[ \mu H_x^2 - \frac{H^2}{2} \left( \mu - \tau \frac{\partial \mu}{\partial \tau} \right) \right] + \frac{\partial}{\partial y} (\mu H_x H_y) + \frac{\partial}{\partial z} (\mu H_x H_z) \quad (1)$$

$$f_y = \frac{\partial}{\partial x} (\mu H_y H_x) + \frac{\partial}{\partial y} \left[ \mu H_y^2 - \frac{H^2}{2} \left( \mu - \tau \frac{\partial \mu}{\partial \tau} \right) \right] + \frac{\partial}{\partial z} (\mu H_y H_z) \quad (2)$$

$$f_z = \frac{\partial}{\partial x} (\mu H_z H_x) + \frac{\partial}{\partial y} (\mu H_z H_y) + \frac{\partial}{\partial z} \left[ \mu H_z^2 - \frac{H^2}{2} \left( \mu - \tau \frac{\partial \mu}{\partial \tau} \right) \right] \quad (3)$$

By dividing the volume density of magnetic field forces in various directions, the magnetic field force  $F$  of the core can be calculated.

$$\begin{aligned} F &= \int_V \vec{f} dV = \vec{i} \int_V f_x dV + \vec{j} \int_V f_y dV + \vec{k} \int_V f_z dV \\ &= \vec{i} \iint \frac{H^2}{2} \left( \mu - \tau \frac{\partial \mu}{\partial \tau} \right) dydz - \vec{j} \iint \frac{H^2}{2} \left( \mu - \tau \frac{\partial \mu}{\partial \tau} \right) dx dz - \vec{k} \iint \frac{H^2}{2} \left( \mu - \tau \frac{\partial \mu}{\partial \tau} \right) dx dy \end{aligned} \quad (4)$$

Based on the above analysis, the magnetostriction force can be simplified:

$$\vec{f} = \frac{1}{2} \nabla \left( H^2 \tau \frac{\partial \mu}{\partial \tau} \right) \quad (5)$$

From the above equation, by solving the variation law between the magnetic permeability  $\mu$  and the bulk density  $\tau$  of the core material, and combining it with the distribution of magnetic field strength  $H$ , the magnetostrictive force of the core can be obtained. However, it is currently difficult to directly solve the vibration caused by the magnetostriction effect through measurement or existing numerical models. Therefore, in engineering applications or simulation calculations, the vibration caused by the magnetostriction effect is generally simplified as material elastic deformation calculation. According to the basic principles of elasticity, for plane strain problems, the magnetostrictive stress can be expressed as follows:

$$\left\{ \begin{array}{l} \sigma = D\varepsilon \\ D = \frac{E}{(1+\nu)(1-2\nu)} \begin{bmatrix} 1-\nu & \nu & \nu \\ \nu & 1-\nu & \nu \\ \nu & \nu & 1-\nu \end{bmatrix} \end{array} \right. \quad (6)$$

Among them,  $\sigma$  is magneto strictive stress,  $D$  is elastic matrix,  $E$  is Young's modulus, and  $\nu$  is Poisson's ratio. Neglecting the influence of damping in the core system, the differential equation of displacement can be obtained:

$$\rho \frac{\partial^2 u}{\partial t^2} = \nabla \cdot \sigma \quad (7)$$

In the above equation,  $u$  is the displacement vector,  $\rho$  is the material density, and  $\sigma$  is stress, which includes stress components in the  $x$ ,  $y$ , and  $z$  directions. In summary, from the above analysis, the components of the magneto strictive force of the transformer core in the  $x$ ,  $y$ , and  $z$  directions can be solved. After converting the solution of the magneto strictive force into an elastic mechanics problem and considering the anisotropy of the ferromagnetic material, the vibration displacement parameters can be obtained by solving the vibration differential equation. In addition, the derivation formula shows that the magneto strictive force of the core is closely related to the distribution of magnetic field strength  $H$ .

## 2.2. Winding Vibration

For point P, based on the principle of symmetry, the sum of the leakage magnetic field vectors of circular coil  $I_1$  in the  $y$ -direction is 0. Therefore, by orthogonally decomposing the leakage magnetic flux  $B_{\sigma y}$ , the radial leakage magnetic flux  $B_{\sigma x}$  and axial leakage magnetic flux  $B_{\sigma z}$  can be calculated as follows:

$$\begin{cases} B_{\sigma x} = \frac{\mu_0 i_{\sigma}}{4\pi} \int_b \frac{l}{(r-x)^2 + y^2 + h^2} \frac{r-x}{\sqrt{(r-x)^2 + h^2}} ds \\ B_{\sigma z} = \frac{\mu_0 i_{\sigma}}{4\pi} \int_{l_i} \frac{l}{(r-x)^2 + y^2 + h^2} \frac{h}{\sqrt{(r-x)^2 + h^2}} ds \end{cases} \quad (8)$$

According to the Ampere force calculation equation  $F = B_{\sigma} I L$ , the axial and radial electromagnetic forces of the winding under sinusoidal fundamental wave can be calculated as follows:

$$\begin{cases} F_x = 2\pi r B_{\sigma x} i(t) = 2\pi r k_z \left\{ I_t I_{ot} \left[ \frac{1 + \cos(2\omega t)}{2} \right] + \sum F_{\sigma x} \right\} \\ F_z = 2\pi r B_{\sigma z} i(t) = 2\pi r k_x \left\{ I_1 I_{\sigma t} \left[ \frac{1 + \cos(2\omega x)}{2} \right] + \sum F_{\sigma z} \right\} \end{cases} \quad (9)$$

Therefore, under the sinusoidal fundamental current, the main frequency of forces in winding is twice the power frequency, 100 Hz, and there is also a portion of the DC component. Meanwhile, due to the vibration of the winding, the pads between turns undergo nonlinear deformation, which can result in the appearance of some 100 Hz harmonic signals in the electromagnetic force, namely,

$$\sum F_x = \sum_{i=1}^k k_i \cos(2k\omega t) \quad (10)$$

## 3. Fixed Structure and Experimental Design

Based on the operation of single-phase transformers in practical engineering, three fixed structures between the core and the transformer tank have been designed. The coil is a continuous coil, and the core is made of a 9 mm stepping, 30QG120 grade silicon steel sheet (Produced by Shougang Group Co., Ltd., Beijing, China). The selection is based on different component combination schemes. The position of the fixed component and the structure of various fixed structures are shown in Figures 1 and 2.

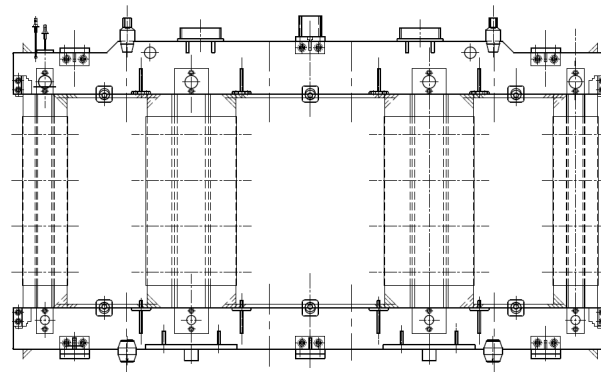


**Figure 1.** Distribution position of single-phase transformer body and fixed structure on it.

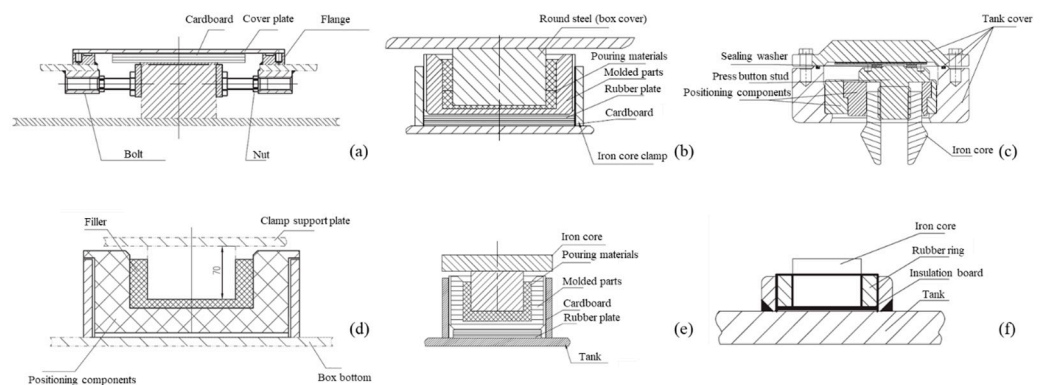


**Figure 2.** Lower fixed structure of the device: (a) upper fixed structure 1; (b) upper fixed structure 2; (c) upper fixed structure 3; (d) lower fixed structure 1; (e) lower fixed structure 2; (f) lower fixed structure 3.

- (1) The nail fixing structure is defined as fixed method 1, which is formed by arranging nuts and bolts on the box cover to form the nail fixing structure. The pressure nail is fixed firmly and reliably on the upper beam of the core strip through a rubber plate;
- (2) The pouring fixed nail structure is defined as fixed method 2, which is formed by pouring fast-drying epoxy resin through the fixed nails on the box cover and the fixed bowl on the core to form a matching fixed structure;
- (3) The eccentric circular fixed nail structure is defined as fixed method 3, which uses bolts to fix the fixed nails and the fixed parts made of hot-pressed polyester laminates to achieve the purpose of upper fixation. The eccentric circular structure can effectively solve the problem of fixed errors.

The experimental transformer is placed in the soundproof laboratory, the measurement points are located on the contour line of the single-phase transformer, with no more than 1 m between each point, as shown in Figure 3. The vibration measurement of the single-phase transformer box adopts the ADLINK USB-2405, which is a 24-bit high-performance dynamic signal acquisition USB module. The vibration sensing module mainly uses piezoelectric acceleration sensors to convert the vibration of single-phase transformers into measurable voltage signals. The noise measurement device is an acoustic imaging instrument, which arranges dozens to thousands of microphones according to a certain pattern and generates the spatial distribution of sound pressure levels through an array of signal processing algorithms.

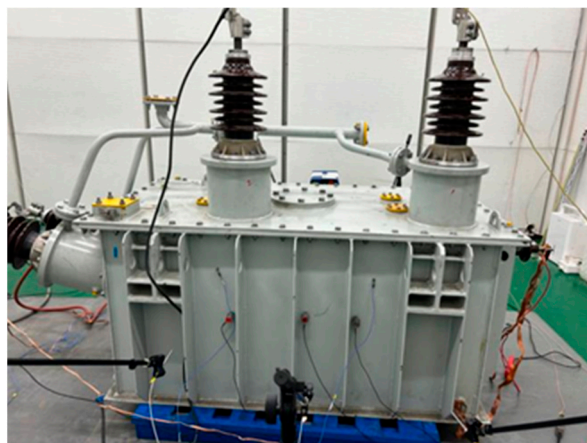


Figure 3. Vibration testing environment and measurement methods for single-phase transformers.

The simulation experiment circuit of harmonic excitation under no-load is shown in Figure 4. The power frequency for the no-load power frequency test is 50 Hz, the secondary winding is open circuit, and the primary winding voltage is 0.9, 0.95, 1, 1.05 times the rated voltage. Harmonic voltage is applied to the transformer through a series combination of a voltage regulator and a test transformer. The harmonic component combinations are 50 Hz + 150 Hz/50 Hz + 150 Hz + 150 Hz + 250 Hz and 50 Hz + 150 Hz + 250 Hz + 350 Hz, respectively. The power frequency for the load frequency test is 50 Hz. The primary winding is short-circuited, the secondary winding is pressurized, and the impedance voltage is 2%. When the secondary side reaches the rated current, the primary side voltage is 161.5 V. The test platform for multi-frequency load testing is the same as that for no-load testing, with frequencies of 50 Hz + 250 Hz/50 Hz + 350 Hz and 50 Hz + 250 Hz + 350 Hz, respectively. The equipment and excitation loading configurations are shown in Tables 1–3.

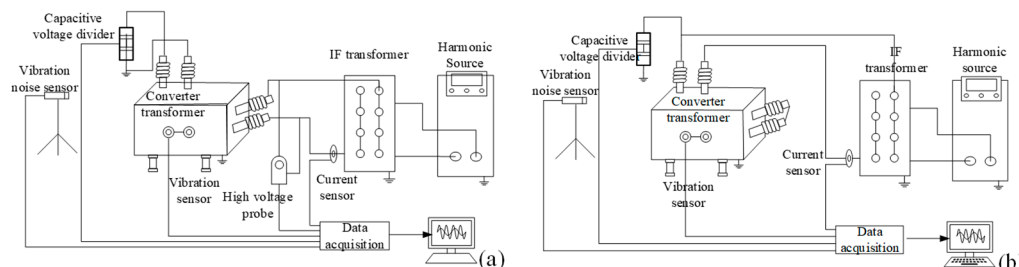


Figure 4. Connection method for no-load test circuit (a); connection method of load test circuit (b).

Table 1. Parameters of test transformers.

	Single Phase Transformer Prototype	Test Transformer t	Three-Phase Voltage Regulator	Intermediate Frequency Transformer	Harmonic Source
Equipment model	ZZD-120/14-5-40	S11-M-100/10	TESGZ-150	S11-M-250	H601D10013
Rated voltage	8.083 kV	10,000/400 V	0~400 V	340 V	0~340 V
Rated capacity	120 kVA	58 kVA	150 kVA	250 kVA	180 kVA

**Table 2.** No load multi-frequency test scheme.

Superposition Frequency Component	Frequency/ Hz	Effective Value of Valve Side Voltage/V	Phase Angle System	Phase Angle Radian System
50 + 150	50	2887	0	0
	150	962	−177.98	−3.10476
50 + 250	50	2887	0	0
	250	577	56.47	0.985088
50 + 350	50	2887	0	0
	350	412	127.58	2.225562
50 + 150 + 250 + 350	50	2887	0	0
	150	962	−177.98	−3.10476
	250	577	56.47	0.985088
	350	412	127.58	2.225562

**Table 3.** Load multi-frequency test scheme.

Superposition Frequency Component	Frequency/ Hz	Effective Value of Valve Side Voltage/V	Phase Angle System	Phase Angle Radian System
50 + 250	50	14.84	20.924	−154
	250	2.97	4.188	121
50 + 350	50	14.84	20.924	−154
	350	2.12	2.989	170
50 + 150 + 250 + 350	50	14.84	20.924	−154
	250	2.12	2.989	170
	350	14.84	20.924	−154

## 4. Results and Discussion

### 4.1. Impact of Harmonic Composition on the Vibration Characteristics of Single-Phase Transformer

Figure 5 shows the vibration characteristic distribution of a single-phase transformer under different harmonic components. The experimental results show that the vibration acceleration amplitude of a single-phase transformer is positively correlated with the injected harmonic voltage and harmonic current. In terms of time-domain performance, after adding various harmonics in the fundamental operating environment, the vibration amplitude of a single-phase transformer increases in proportion to the harmonic content, resulting in a denser spectrum, but clearer patterns cannot be read. In terms of frequency spectrum distribution, the addition of a third harmonic, fifth harmonic, and seventh harmonic affects the distribution ratio of vibration characteristics at 300 Hz, 500 Hz, and 700 Hz, respectively, while also excessively high the amplitude of the fundamental frequency spectrum. This is because each harmonic not only affects the natural vibration frequency of the core and winding but also causes resonance between component structures, resulting in an overall increase in the amplitude of vibration characteristics. This is particularly evident when the fundamental wave and the third, fifth, and seventh harmonics operate together. Due to the decrease in the content and amplitude of the third, fifth, and seventh no-load harmonic voltages, as well as the fifth and seventh load harmonic currents in single-phase transformers, the vibration acceleration amplitudes of the third, fifth, and seventh harmonic voltages and currents superimposed on the fundamental wave measured in the experiment also decreased sequentially. The main vibration frequency of single-phase transformers does not change much, all within the range of 0–500 Hz. In the no-load test, when the fundamental wave is superimposed with the third, fifth, and seventh harmonic

voltages, the acceleration amplitude is maximum, and the main frequency of single-phase transformer vibration significantly increases between 0 and 1500 Hz. In the load test, the maximum acceleration amplitude was obtained by superimposing the fifth and seventh harmonic currents of the fundamental wave, and the main frequency of the single-phase transformer vibration did not significantly increase.

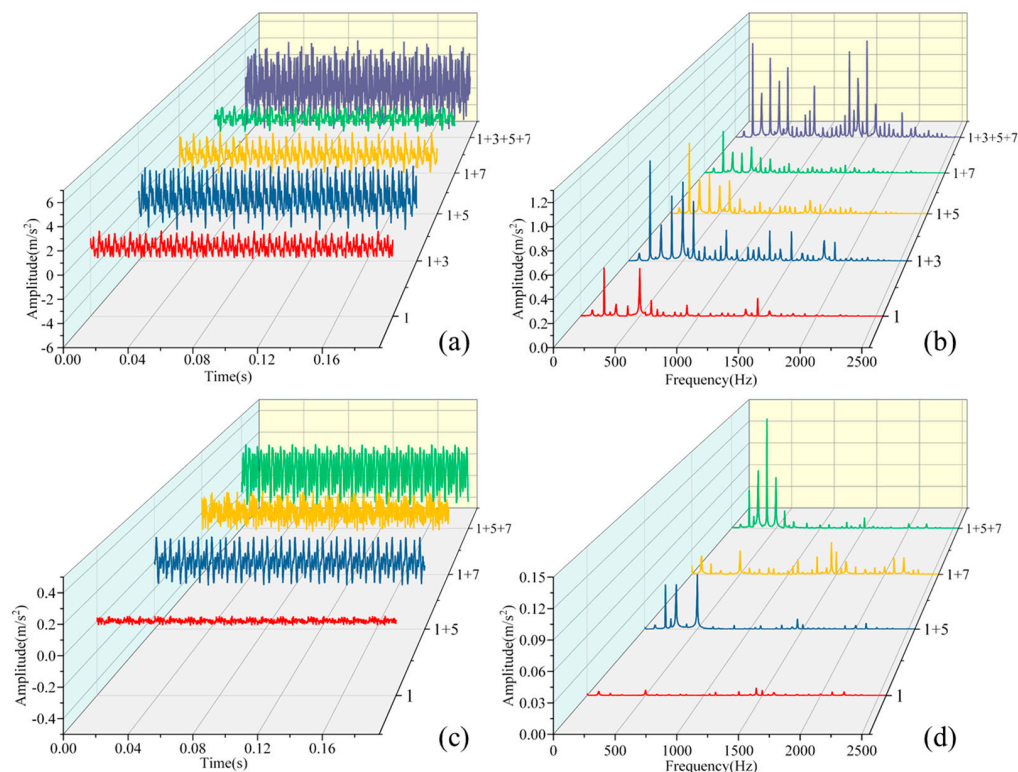


**Figure 5.** Distribution of vibration characteristics under different harmonic components: (a) no-load time domain; (b) Empty frequency domain; (c) Load time domain; (d) Load time domain.

Comparing the data in Figure 6, when loaded with power frequency, the maximum vibration acceleration value of the transformer tank is  $0.04 \text{ m/s}^2$ . When the fifth and seventh harmonics are added, the maximum vibration acceleration value is  $0.25 \text{ m/s}^2$ , and the vibration acceleration is 5.7 times that of the power frequency. When the power frequency is unloaded, the maximum vibration acceleration value of the transformer tank is  $1.38 \text{ m/s}^2$ . When the third, fifth, and seventh harmonics are added, the maximum vibration acceleration value of the transformer tank surface is  $5.29 \text{ m/s}^2$ , and the amplitude of the vibration acceleration is 3.8 times that of the power frequency.

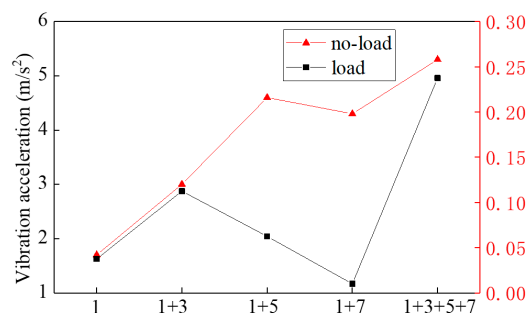


**Figure 6.** Comparison of vibration characteristics of no load under different harmonics.



Through the discrete Fourier transform of the vibration signal, under no-load power frequency, the vibration acceleration spectrum is mainly concentrated below 500 Hz, with low-frequency vibration being the main component. After adding harmonics, the vibration characteristics change. The spectral distribution range of the vibration expands, causing the appearance of high-frequency components. The energy proportion of each frequency band of the vibration changes. With the injection of harmonics, the amplitude of the high-frequency component of the transformer vibration increases, and the vibration intensity significantly increases when the transformer vibrates at high-order natural frequencies.

#### 4.2. Impact of Fixed Method on the Vibration Characteristics of Single-Phase Transformer

Figure 7 shows the distribution of surface vibration characteristics under different fixed structures under no-load conditions. From the time-domain graph 7a, the vibration acceleration amplitude of fixed method 2 is the lowest under no-load conditions, which is because the vibration of single-phase transformers under no-load conditions mainly comes from the iron core. At present, the core lamination process is relatively advanced, which makes the Maxwell force between silicon steel sheets relatively negligible. Therefore, the vibration of the core mainly comes from the axial magnetostriction effect. The advantage of pouring positioning lies in its ability to effectively stabilize the vertical forces acting on the body. At the same time, compared to the rigid material of the positioning nail, epoxy material has a stronger buffering effect.

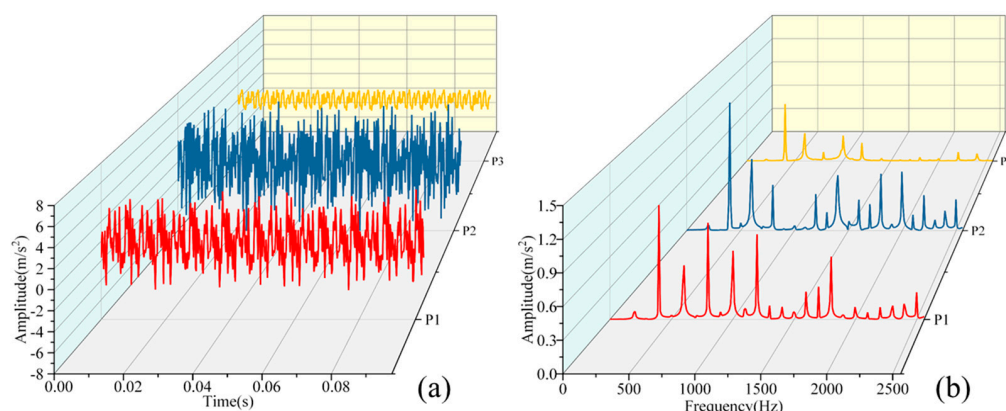
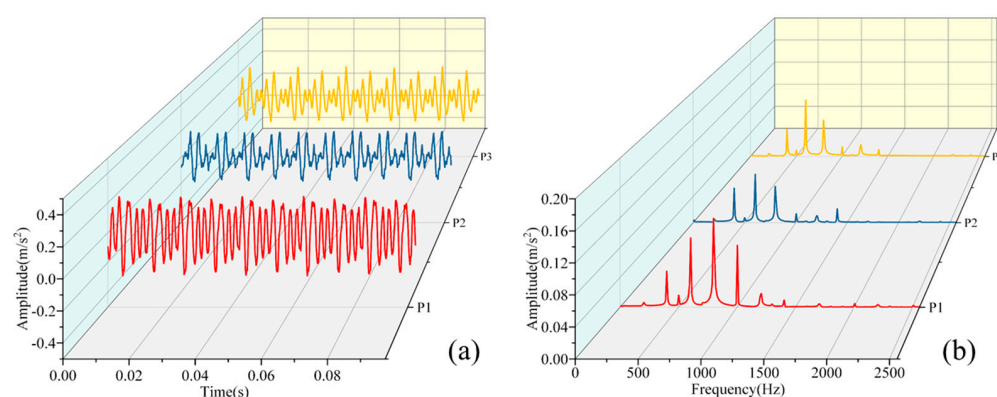


**Figure 7.** Time–frequency domain waveforms of no-load harmonic vibration acceleration for three fixed structures: (a) time domain; (b) frequency domain.

Figure 7a shows the frequency domain distribution of vibration under different fixed modes, the vibration frequency domain distribution of single-phase transformers under different fixed modes under no-load conditions was obtained. The main frequency of vibration acceleration under no-load conditions remains basically unchanged for different fixed methods, while the distribution of secondary frequencies varies. However, the main distribution of secondary frequencies for all three methods is within 1000 Hz. The amplitude of the secondary frequency within 1000 Hz under fixed method 1 is greater than the other two fixed methods, and there are still higher secondary frequencies outside 1000 Hz, indicating that fixed method 1 has the worst suppression effect on core resonance. The best performance of the vibration frequency domain distribution characteristics of the three under no-load conditions is fixed method 3, which has the most significant suppression effect on resonance at high frequencies, but its overall amplitude is larger than fixed method 2. The most reasonable explanation here is that fixed method 2 has the least and smallest low-frequency harmonics. Even though there are more high-frequency harmonics under fixed method 2, the overall component of transformer vibration at high frequencies is relatively small, and the maximum contribution of the vibration effect still

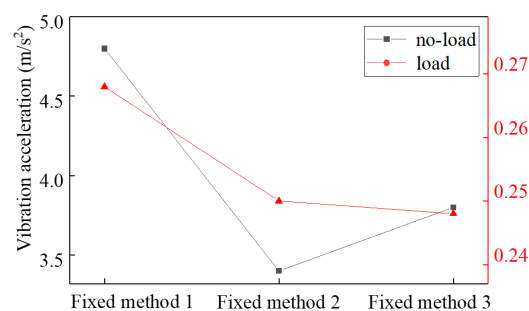
needs to focus on low-frequency harmonics. Therefore, comparing the performance of the three fixed methods under no-load conditions, the pouring fixed nail structure is the best, with a vibration acceleration amplitude reduced by about 10% compared to fixed method 1.

Figure 8 shows the distribution of surface vibration characteristics of transformer tanks under different fixed structures under load conditions. From graph 8a under load conditions, the vibration acceleration amplitudes of fixed mode 2 and fixed mode 3 are similar, with the optimal one shown as fixed mode 3. Under load conditions, the vibration mainly comes from the windings, and the displacement of the windings is mainly reflected in the radial changes. This result reflects the unique role of the eccentric circle positioning method, which has an additional effect on the radial fixation of the transformer body. From Figure 2c,f of the eccentric circle design, it can be seen that the asymmetric eccentric circle design of the eccentric circle can ensure good stability of the device body under the trend of left, right, or rotating motion. From Figure 8b of the frequency domain distribution of single-phase transformer vibration under load conditions, the frequency domain distribution of single-phase transformers under fixed mode 2 and fixed mode 3 is cleaner, which means that the resonance effect is reduced.



**Figure 8.** Time–frequency domain waveform of load harmonic vibration acceleration for three fixed structures: (a) time domain; (b) frequency domain.

To visually summarize and compare the merits of the fixed methods, the vibration amplitudes under different operating conditions are plotted on the double y-axis dotted line graph shown in Figure 9. Overall, fixed method 2 has the most advantage under no-load harmonic conditions, while it is slightly inferior to fixed method 3 under load conditions, and the performance of fixed method 3 under comprehensive conditions is relatively stable. Fixed method 1 has the maximum vibration amplitude under any operating condition.



**Figure 9.** Comparison of vibration characteristics of three fixed structures considering harmonics.

By placing a microphone sensor 0.6 m away from the horizontal axis of the single-phase transformer body, the noise of different fixed single-phase transformers under no-load harmonic conditions was measured, compared, and measured. The time–frequency domain of

sound pressure of each fixed method is plotted in Figures 10 and 11. The noise performance under no-load multi-frequency conditions is consistent with the vibration law, and the sound pressure amplitude is shown as fixed method 1 > fixed method 3 > fixed method 2. The sound pressure spectrum range is mainly between 200 Hz and 800 Hz. Under multi-frequency load conditions, the amplitude of sound pressure shows fixed mode 1 > fixed mode 2 > fixed mode 3, and the frequency spectrum range of sound pressure is mainly between 200 Hz and 1000 Hz.

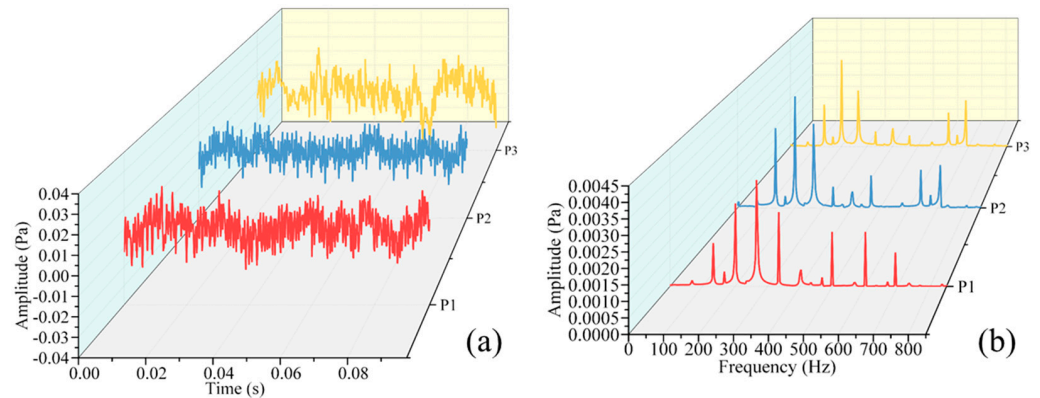


**Figure 10.** Time–frequency domain waveforms of sound pressure for three fixed structures under no load conditions: (a) time domain distribution; (b) frequency domain distribution.

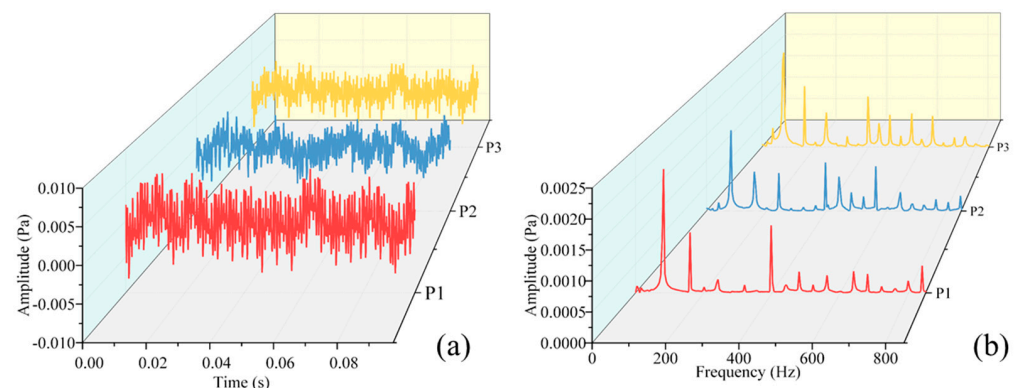


**Figure 11.** Time–frequency domain waveforms of sound pressure for three fixed structures under load conditions: (a) time domain; (b) frequency domain.

To quantitatively compare the contributions of three fixed methods in noise suppression more intuitively, the sound pressure data of single-phase transformers under different fixed methods were converted into sound pressure levels and plotted in Figure 12. Under no-load multi-frequency conditions, compared with the pressure nail fixed structure, the use of pouring fixed nail fixed structure can reduce about 2.3 dB. Under multi-frequency load conditions, using an eccentric circular fixed nail structure can reduce the noise by about 3.3 dB. Therefore, it can be clearly stated that in terms of noise control, the poured fixed structure performs the best and most stable under different working conditions.

Compared with previous research on transformer noise reduction measures, the fixed method does not have the greatest effect on suppressing vibration. Under the optimal combination form, only 2–3 dB noise reduction can be achieved (generally, optimizing the structure of the core and winding can achieve 5 dB noise reduction). However, it is worth noting that the design and manufacturing cost of fixed components is much lower than that of iron cores and windings, so this value is still fully worthy of industry attention. On the other hand, the fixed component body is not powered, which means that there are fewer factors to consider in the design, such as safety margin and operating conditions, and only

appropriate modal parameters and stray loss parameters need to be designed. Overall, from the perspectives of economy, design and preparation difficulty, and wide industrial application effects, fixed method optimization is undoubtedly the preferred choice for suppressing vibration and noise in single-phase transformers.

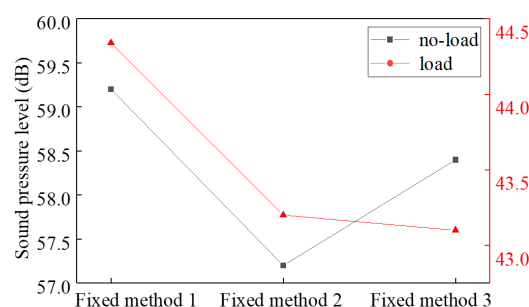


**Figure 12.** Comparison of sound pressure characteristics of three different fixing methods under different working conditions.

## 5. Conclusions

- (1) Impact of harmonic frequency on the vibration of single-phase transformers: during load operation, the amplitude is  $1 + 5 > 1 + 3 > 1 + 7$ ; when running without load, the amplitude is  $1 + 3 > 1 + 5 > 1 + 7$ ;
- (2) Under no-load multi-frequency conditions, amplitude fixing method 1 > fixing method 3 > fixing method 2;
- (3) Under multi-frequency load conditions, the vibration amplitude follows the fixed method 1 > fixed method 2 > fixed method 3;
- (4) The pouring fixed nail structure can reduce vibration amplitude by about 10% and noise by about 2.5 dB.

Therefore, in the noise reduction design of industrialized single-phase transformers, different fixing methods can be considered according to their importance: if winding noise reduction is the focus, eccentric circular fixing nails should be used to fix the structure; if noise reduction in the core is the focus, a cast type fixing nail structure should be used for fixation; When there is no specific noise reduction area, it is recommended to use pouring type fixing nails to fix the structure. The above conclusion applies to the optimization of single-phase transformer fixing methods for vibration and noise characteristics.

**Author Contributions:** Conceptualization, L.Z. (Li Zhang) and L.Z. (Liang Zou); software, Y.S. (Yupu Sun); validation, Y.S. (Yupu Sun); formal analysis, Y.S. (Youliang Sun); investigation, Y.S. (Youliang Sun); resources, Y.S. (Youliang Sun); data curation, L.Z. (Li Zhang); writing—original draft preparation, Y.S. (Youliang Sun); writing—review and editing, H.W.; visualization, Y.S. (Yupu Sun); supervision, L.Z. (Li Zhang); project administration, L.Z. (Liang Zou); funding acquisition, Y.S. (Youliang Sun). All authors have read and agreed to the published version of the manuscript.

**Funding:** Key R&D Program of Shandong Province (2021CXGC010210).

**Data Availability Statement:** Data are contained within the article.

**Conflicts of Interest:** Authors Youliang Sun and Yupu Sun are employed by Shandong Power Equipment Company Limited. The remaining authors declare that the research was conducted in the absence of any commercial or financial relationships that could be construed as a potential conflict of interest.

## References

1. Kim, C.K.; Sood, V.K.; Jang, G.S.; Lim, S.J.; Lee, S.J. *HVDC Transmission: Power Conversion Applications in Power Systems*; Wiley-IEEE Press: Hoboken, NJ, USA, 2009.

2. Wang, H.; Zhang, L.; Sun, Y.; Zou, L. Research on the influence mechanism of harmonic components on the noise distribution characteristics of converter transformers. *Int. J. Electr. Power Energy Syst.* **2024**, *160*, 110095. [[CrossRef](#)]
3. Du, B.; Wang, Q.; Tu, Y.; Tanaka, Y.; Li, J. Guest Editorial: Advanced Materials for HVDC Insulation. *High Volt.* **2020**, *5*, 351–352.
4. Kumar, N. EV Charging Adapter to Operate with Isolated Pillar Top Solar Panels in Remote Locations. *IEEE Trans. Energy Convers.* **2024**, *39*, 29–36. [[CrossRef](#)]
5. QLi, Q.; Ladislav, N.E.; Huang, X.; Liu, Q.; Wang, Z. Research Advances of Bubble Dynamics in Power Transformers. *CSEE J. Power Energy Syst.* **2024**, *10*, 2639–2656.
6. Saha, J.; Kumar, N.; Panda, S.K. Adaptive Grid-Supportive Control for Solar-Power Integrated Electric-Vehicle Fast Charging Station. *IEEE Trans. Energy Convers.* **2023**, *38*, 2034–2044. [[CrossRef](#)]
7. Kumar, N.; Saxena, V.; Singh, B.; Panigrahi, B.K. Power Quality Improved Grid-Interfaced PV-Assisted Onboard EV Charging Infrastructure for Smart Households Consumers. *IEEE Trans. Consum. Electron.* **2023**, *69*, 1091–1100. [[CrossRef](#)]
8. Wang, H.; Zhang, L.; Sun, Y.; Zou, L. Finite Element Simulation and Experimental Study on Vibration Characteristics of Converter Transformer Under DC Bias. *Prot. Control. Mod. Power Syst.* **2024**, *9*, 110–125. [[CrossRef](#)]
9. Lian, Y.; Wang, J.; Li, Z.; Huang, L.; Jiang, X. Residual attention guided vision transformer with acoustic-vibration signal feature fusion for cross-domain fault diagnosis. *Adv. Eng. Inform.* **2025**, *64*, 103003. [[CrossRef](#)]
10. Zhao, Y.; Crossley, P. Impact of dc bias on differential protection of converter transformers. *Int. J. Electr. Power Energy Syst.* **2020**, *115*, 105426. [[CrossRef](#)]
11. Liu, X.; Wu, J.; Jiang, F.; Wang, Y.; Zhang, C.; Hui, Y. Electromagneto-mechanical numerical analysis and experiment of transformer influenced by DC bias considering core magnetostriction. *J. Mater. Sci. Mater. Electron.* **2020**, *31*, 16420–16428. [[CrossRef](#)]
12. Yang, J.; Zhang, G.; Tian, Z.; Stewart, E.; Liu, Z. Early-Stage Electrical Fault Identification for Traction Transformers Using Vibration Signals Based on Dual-Attention Convolutional Network. *IEEE Trans. Ind. Cyber-Phys. Syst.* **2024**, *2*, 471–483. [[CrossRef](#)]
13. Yadav, S.; Mehta, R.K. Modelling of magnetostrictive vibration and acoustics in converter transformer. *IET Electr. Power Appl.* **2021**, *15*, 332–347. [[CrossRef](#)]
14. Mohan, M. A comprehensive review of DC fault protection methods in HVDC transmission systems. *Prot. Control Mod. Power Syst.* **2021**, *6*, 1.
15. Han, P.; Tong, Q.; Wang, Y.; Chen, Z.; Yang, W.; Hu, D.; Wu, H.; Zhang, J. An Inrush Current Suppression Strategy for UHV Converter Transformer Based on Simulation of Magnetic Bias. *IEEE Trans. Power Del.* **2022**, *37*, 5179–5189. [[CrossRef](#)]
16. Shao, P.; Luo, L.; Yong, L.; Rehtanz, C. Electromagnetic Vibration Analysis of the Winding of a New HVDC Converter Transformer. *IEEE Trans. Power Deliv.* **2011**, *27*, 123–130. [[CrossRef](#)]
17. Zhao, X.; Envelope ZS, P.; Zhang, Y.; Liu, Z. Research on design method of metamaterial sound field control barrier based on transformer vibration and noise. *Energy Rep.* **2022**, *8*, 1080–1089. [[CrossRef](#)]
18. Peng, X.; Shan-Ming, W.; Xiang-Heng, W. Study of harmonic suppression scheme based on three-winding transformer. *Adv. Technol. Electr. Eng. Energy* **2005**, *24*, 41–43.
19. Zhihua, P. Magnetic field simulation and no-load loss calculation of large three-phase five-column disassembled transformer. In Proceedings of the 2021 International Conference on Intelligent Computing, Automation and Systems, Chongqing, China, 29–31 December 2021; pp. 466–469.
20. Li, W.; Zhou, L.; Chen, J.; Liu, B.; Gao, S.; Zhang, C.; Wang, D. Numerical Model for Eddy-Current Loss of Wound Core in Single-Phase Transformer. *IEEE Trans. Transp. Electrification* **2024**, *10*, 150–162. [[CrossRef](#)]
21. Ji, L.; Ya-Qian, H.E.; Kai, L.I. The Multi-physics Research on Iron-Core Vibration Noise of Power Reactor. *J. Harbin Univ. Sci. Technol.* **2017**, *22*, 35–40.
22. Wang, Z.; Li, J.; Sofian, D.M. Interpretation of Transformer FRA Responses—Part I: Influence of Winding Structure. *IEEE Trans. Power Deliv.* **2009**, *24*, 703–710. [[CrossRef](#)]
23. Wu, S.; Ji, S.; Zhang, Y.; Wang, S.; Liu, H. A Novel Vibration Frequency Response Analysis Method for Mechanical Condition Detection of Converter Transformer Windings. *IEEE Trans. Ind. Electron.* **2024**, *71*, 8176–8180. [[CrossRef](#)]
24. Chen, H.; Zheng, Z.; Xiao, J. Determining the Number of Transformer Shielding Winding Turns for Suppressing Common-Mode Noise in Flyback Converters. *IEEE Trans. Electromagn. Compat.* **2017**, *60*, 1606–1609. [[CrossRef](#)]
25. Zhu, L.; Hao, J.; Lu, L. Research on Influence of Damping on the Vibration Noise of Transformer. *IEEE Access* **2022**, *10*, 92128–92136. [[CrossRef](#)]
26. He, S.; Huang, D.; Feng, X.; Deng, J.; Li, J.; Zhu, J. Transient potential distribution on transformer winding considering the effect of core lamination stack. *AIP Adv.* **2020**, *10*, 015024. [[CrossRef](#)]
27. Moses, A.J.; Anderson, P.I.; Phophongviwat, T. Localized Surface Vibration and Acoustic Noise Emitted from Laboratory-Scale Transformer Cores Assembled from Grain-Oriented Electrical Steel. *IEEE Trans. Magn.* **2016**, *52*, 1–15. [[CrossRef](#)]
28. Barros, R.; Costa, E.; Araujo, J.F.; de Andrade, F.L.; Ferreira, T.V. Contribution of inrush current to mechanical failure of power transformers windings. *High Volt.* **2019**, *4*, 300–307. [[CrossRef](#)]

29. Zhu, W.B.; Du, B.X.; Li, J.; Jiang, J.P.; Su, J.G.; Li, A.; He, Z.Y.; Zhang, M.M.; Huang, P.H. Effects of Temperature on Surface Charge Behavior of Fluorinated Oil-impregnated Paper under the Coupling of DC and Pulse Voltages. In Proceedings of the 2018 IEEE 2nd International Conference on Dielectrics, Budapest, Hungary, 1 July 2018.
30. Li, Y.; Yang, Z.; Zhang, C.; Mu, S. Vibration and Noise Measurement of Medium-High Frequency Transformer Cores Under Non-Sinusoidal Excitation. *IEEE Trans. Magn.* **2022**, *58*, 1–5. [[CrossRef](#)]
31. Weiser, B.; Pfutzner, H.; Anger, J. Relevance of Magnetostriction and Forces for the Generation of Audible Noise of Transformer Cores. *IEEE Trans. Magn.* **2000**, *36*, 3759–3777. [[CrossRef](#)]
32. Cao, C.; Xu, B.; Li, X. Monitoring Method on Loosened State and Deformational Fault of Transformer Winding Based on Vibration and Reactance Information. *IEEE Access* **2020**, *8*, 215479–215492. [[CrossRef](#)]
33. He, J.; Yu, Z.; Zeng, R.; Zhang, B. Vibration and Audible Noise Characteristics of AC Transformer Caused by HVDC System Under Monopole Operation. *IEEE Trans. Power Deliv.* **2012**, *27*, 1835–1842. [[CrossRef](#)]

**Disclaimer/Publisher’s Note:** The statements, opinions and data contained in all publications are solely those of the individual author(s) and contributor(s) and not of MDPI and/or the editor(s). MDPI and/or the editor(s) disclaim responsibility for any injury to people or property resulting from any ideas, methods, instructions or products referred to in the content.